Statistical mechanical modeling of catalytic polymerization within surface-functionalized mesoporous materials

Da-Jiang Liu,[1] Hung-Ting Chen,[1,2] Victor S.-Y. Lin,[1,2] and J. W. Evans[1,3]
[1]*Ames Laboratory-U.S. DOE, Iowa State University Ames, Iowa 50011, USA*
[2]*Department of Chemistry, Iowa State University, Ames, Iowa 50011, USA*
[3]*Department of Mathematics, Iowa State University, Ames, Iowa 50011, USA*
(Received 28 January 2009; revised manuscript received 6 May 2009; published 6 July 2009)

A discrete lattice model is developed to describe diffusion-mediated polymerization occurring within mesopores, where reaction is enhanced at catalytic sites distributed within the interior of the pores. Diffusive transport of monomers and polymers is one-dimensional, diffusion coefficients for the latter decreasing with polymer length. Kinetic Monte Carlo simulation is utilized to analyze model behavior focusing on a "clogging" regime, where the amount of polymer within the pores grows. We characterize the evolution of the overall and mean length of polymers, the mean number of polymers, as well as the polymer spatial and length distributions.

DOI: 10.1103/PhysRevE.80.011801 PACS number(s): 82.35.−x, 68.65.−k, 82.75.Qt

I. INTRODUCTION

There has been considerable interest for more than one decade in the utilization of mesoporous materials to facilitate production and processing of polymeric materials with desired higher-order structures [1], e.g., linear "molecular wires" versus more complex cross-linked networks. Such a capability would avoid the need for post-processing steps often required for traditional polymerization approaches. Mesoporous materials composed of silica or other oxides can be fabricated with hexagonal close-packed arrays of parallel nanopores and with typical diameters ranging from 2 to 10 nm [2]. These materials provide supports for polymerization catalysts [1], where ideally the catalytic sites should be distributed within the pores. Previous studies have utilized mesoporous catalytic materials for the polymerization of ethylene, propylene, methylmethacrylate, lactones, alkynes, 1,4-diethynylbenzene, etc.; the latter forming poly(phenylene butadyiene) or PPB. See, for example, [1,3–5].

One general issue is characterization of the possible "modes of operation" of these nanoscopic reactors or polymer processing machines. One might anticipate operation in either extrusion or "clogging" modes depending on the reaction conditions, the details of the polymerization mechanism, the distribution of catalytic sites, etc. For the polymerization of ethylene using mesoporous silica fibers (MSF) as the catalyst support, polymers were extruded from adjacent pores and then spontaneously agglomerated to produce crystalline polyethylene fibers [6]. This process is somewhat analogous to biosynthesis of crystalline cellulose through nanopores in a cellular membrane [6,7]. At the other extreme, the polymers could primarily remain within the pores due to various factors such as low mobility or their intrinsic low solubility. In this regime, the polymers clog the pores of the mesoporous material which could lead to the fabrication of silica/functional polymer nanocomposite materials [1].

The current modeling study was motivated primarily by experiments demonstrating the successful fabrication of linear molecular wires of PPB encapsulated within a Cu^{2+}-functionalized MCM-41 silica, a mesoporous silica nanosphere (MSN) material [5]. The key to this success was application of a co-condensation procedure [8] which resulted in the copper catalyst sites being distributed "homogeneously" within the pores. In contrast, direct grafting followed by impregnation methods led to catalytic sites distributed on the exterior surface of the nanospheres and partly in the pore interiors near the channel openings. Presumably, for MCM-41 silica functionalized with the co-condensation method, alignment of monomers and the resulting polymers within the pores facilitates development of molecular wires. Under typical reaction conditions in this system, polymers tend to clog the pores rather than be extruded. These experiments prompt some fundamental questions and challenges with regard to understanding how the rate and extent of polymerization depend on: (i) the amount and spatial distribution of catalytic sites, (ii) the diffusion rate and spatial distribution of monomers, and (iii) the diffusivity of polymers.

Since the transport of monomers and PPB polymers occurs inside MCM silica mesopores with a small diameter of 2.5 nm in these experiments [5], one expects that diffusion may exhibit some anomalous features associated with one-dimensional (1D) or "single-file" systems. Issues pertaining to anomalous transport, particularly microporous zeolite materials, have been studied extensively both from applied and from fundamental statistical mechanical perspectives [9–12]. However, for the polymerization process of interest here, there is a broader and more substantial challenge of elucidating the interplay between one-dimensional transport and the reaction kinetics [13–15]. To make some progress in this direction, it is appropriate to first consider somewhat idealized models for the process of interest. These models must incorporate the one-dimensional transport of monomers and polymers within pores, an appropriate distribution of catalytic sites within pores, and the catalyzed polymerization kinetics. They should predict the resulting polymer length and location distributions and related quantities. For convenience, we shall implement these processes in a discretized lattice model where cooperative reaction-diffusion behavior can be readily analyzed via kinetic Monte Carlo (KMC) simulation [16–18].

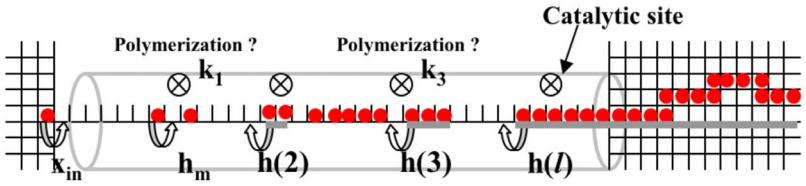

FIG. 1. (Color online) Schematic of lattice-gas model for polymerization within a mesopore indicating both transport and reaction kinetics.

In Sec. II, we describe in detail our discrete model for polymerization. A variety of simulation results are presented in Sec. III for the diffusion-limited polymerization regime. We focus on dependence of the total amount of polymerization on the monomer input rate in Sec. III A, the dynamics of growth of the average polymer length in Sec. III B, and on the complete polymer length distribution in Sec. III C. Selected results for other regimes and different model parameters are presented in the Sec. IV. Finally, conclusions are provided in Sec. V.

II. LATTICE-GAS MODEL FOR POLYMERIZATION

A. Model spatial structure

Our selection of model parameters is partly guided by the polymerization of PPB within Cu^{2+}-functionalized MCM-41 silica [5]. Here, the pore diameter is $d \sim 2.5$ nm and the pore length is of the order of $L \sim 200$ nm. The catalytic sites are distributed along the interior of the pore with a mean separation of $l_c \sim 10$ nm. The monomer is $l_m \sim 1.03$ nm long (and ~ 0.5 nm wide). Given that the monomer length, l_m, is significantly smaller than the other characteristic length scales (l_c and L), it is natural to utilize a lattice-gas model framework where each monomer occupies a single site on a linear one-dimensional lattice within each mesopore. Polymer segments within each pore occupy multiple adjacent sites on this lattice. We treat diffusion of monomers and polymer segments within the pore as one dimensional, involving hopping between adjacent sites on this linear lattice (see below). This lattice can be regarded as expanding to a three-dimensional (3D) structure outside of the pore to allow description of the monomer distribution and polymer configurations in the surrounding fluid. However, the key model dynamics will occur on the 1D lattice within the pore. We will augment this dynamics with a simplified description of monomer input from the fluid. We could also account in a simple way for the effect of any reduced polymer solubility outside (relative to within) the pore which would inhibit extrusion and for the greater configurational entropy of polymers outside the pore which might enhance extrusion (see Fig. 1).

B. Model dynamics

In this modeling, we will assume the same solubility within and outside the pore for monomer and polymer species. In this case, the key components of the model dynamics are as follows:

(i) Monomer input to the pore. Monomers are assumed to be randomly distributed in solution outside of the mesoporous silica nanospheres including on the sites adjacent to the ends of the pore, provided that such sites are not occupied by a partly extruded polymer chain (cf. the right pore end in Fig. 1). Population of these end sites provides a source of monomers to the interior of the pore. We assume a constant rate of input, x_{in}, of monomers to empty sites just inside the pore, where x_{in} is proportional to the above exterior monomer population.

(ii) Monomer diffusion. Monomers undergo diffusive hopping to adjacent sites on the linear lattice within the pore at rate h_m, provided those sites are not occupied by another monomer or part of a polymer. The rate h_m also applies for hopping from the end sites within the pore to the sites immediately outside the pore, for which the reverse process is controlled by the rate x_{in}.

(iii) Polymer diffusion. Once polymers of length l are formed (see below) which reside within the pore, they hop diffusively, shifting their position by one site (to the left or right) at rate $h(l)$. In general, one expects reduced diffusivity with increasing polymer length, i.e., $h(l)$ decreases with increasing l. This feature will significantly reduce the rate of extrusion of polymers from the pore. In the current modeling, we will assume that $h(l)=h_m/l^n$, where we treat (integer) n as a free parameter and assess how polymerization kinetics depends on its value. Furthermore, we will also apply this rate when one end of the polymer is outside the pore. However, polymers completely outside the pore cannot re-enter. Analyses of polymer diffusion in random porous media [19,20] predict size scaling of the diffusion coefficient with a variety of values of n depending on the detailed dynamics. Results can deviate from the simple Rouse-like behavior, $h(l) \sim l^{-1}$, or $h(l)^{-1.8}$ if hydrodynamics plays a role. Polymer diffusion behavior in confined mesopore environments is not fully characterized. It is plausible that interaction with the mesopore could produce a complex l dependence of $h(l)$ [21] and that concerted many-particle diffusive dynamics could be present [22]. However, such possibilities are not included in our modeling.

(iv) Polymerization. When two monomers sit on an adjacent pair of sites directly below a catalytic site, polymerization to form a dimer occurs at rate k_1. Likewise, when a monomer and the end of a dimer or longer polymer are on adjacent sites below a catalytic site, polymerization occurs at rate k_2. When the ends of two polymers are on adjacent sites below a catalytic site, further polymerization occurs at rate k_3. In the benchmark studies in this work, we consider only the special case $k_1=k_2=k_3(=k$, say) and focus on the regime $k \to \infty$, i.e., rapid polymerization occurring immediately monomers and/or the ends of polymers reach adjacent sites below catalytic sites. This corresponds to the regime of diffusion-limited polymerization.

Finally, we offer some additional comments related to polymer nanoextrusion. Once polymers are formed within the pore, they continue to diffuse and thus can potentially

leave the pore. However, any continued polymerization for a polymer partly outside the pore would increase its length and further reduce its diffusivity. In the benchmark simulations in this work, we regard a polymer of any length $l \geq 2$ as remaining perfectly linear when it partly exits the pore and assign equal hop rates of $h(l)$ for hopping further out of the pore or back into the pore. In fact, PPB polymers are quite stiff so that this is a reasonable assumption. Once the polymer completely exits the pore, we propose that it cannot return due to orientational misalignment. When a polymer is partly out of the pore, it blocks the site adjacent to the end of the pore from being populated by a monomer and thus blocks monomer input to that end of the pore.

More generally, one might expect that the partly extruded portion of the polymer in the fluid has greater configurational entropy then the portion which is configurationally constrained inside the pore. Then, there is an entropic driving force for extrusion. Rather than incorporate a detailed treatment of polymer configurations in the fluid, one could adopt simple Markov model, where the probability for a bend in the portion of the polymer in the fluid equals p (per site). One might further assume that if such a bend occurs at the site in the fluid adjacent to the end of the pore, then diffusive hopping of the polymer back into the pore is blocked. Thus, for a partly extruded polymer, the probability of hopping back into the pore would be reduced to $1-p$ relative to that for hopping further out, so its dynamics would be described by biased diffusion on a linear lattice. However, below we set $p=0$ (unbiased diffusion). Again the justification is that PPB polymers are quite stiff. The propensity for clogging of pores in this system also indicates the lack of a strong driving force for extrusion.

The model dynamics is analyzed by the lattice-gas KMC simulation approach. The algorithm is a combination of the standard method and the n-fold rejection-free method to reach a balance between algorithmic efficiency and bookkeeping overhead cost. Results presented in the following sections are obtained from extensive simulation data. Typically, each data point is the average over 10^4 KMC runs, thus the statistical uncertainty is around 1%, assuming normal distributions. The quality of the data is also evidenced by the smooth curves interpolating data points.

III. DIFFUSION-LIMITED POLYMERIZATION: SIMULATION RESULTS

In this section, we consider exclusively the case of diffusion-limited polymerization with $k=\infty$. We set $h_m=1$ which in effect takes the characteristic time for monomer hopping, $\tau_m=1/h_m(=1)$, as our unit of time. (This time unit corresponds to the physical time for the mean-square displacement of a diffusing monomer to equal the square of length of the monomer.) The monomer length, l_m, is taken as our unit of length and the length of the pores is chosen as $L=200$ (unless stated otherwise). There are on average 20 catalytic sites randomly distributed within the pore, so their average separation is $l_c \approx 10$. The exponent describing the decrease in polymer diffusivity with increasing length is varied from $n=1$ to $n=4$. Note that in the absence of polymerization, the equilibrium concentration per site of monomers within the pore would equal $c_{eq}=x_{in}/(h_m+x_{in}) \approx x_{in}/h_m$ for small x_{in} (so that $c_{eq} \approx x_{in}$ for $x_{in} \ll 1$ choosing $h_m=1$). This result reflects a balance between the input rate of monomers to the end site within the pore, $x_{in}(1-c_{eq})$, with the exit rate $h_m c_{eq}$.

For the typical choices of x_{in} used in our study of 0.01 or above, the polymerization process is found to operate essentially in a clogging regime where the amount of polymer within the pore slowly increases. Evolution with reaction time of the polymer and monomer distributions within an ensemble of pores is shown in Fig. 2 for various $n=1-4$. Each frame in the figure is a composite plot of simulation results for 27 separate pores. These are combined into a single image representative of an array of pores within an MSN or MCM-41 material. In all cases, there is a tendency for polymers to form near the ends of the pore since initially, the monomer density is higher in that region. The formation of polymers blocks additional monomers from reaching the interior of the pore, so the monomer density in that interior region will decrease. As reaction time increases, smaller polymers aggregate into larger ones, with polymer growth continues to be fed by input of monomers at the ends of the pore. In this work, we will focus on the distribution of polymers within the pore rather than extrusion of polymers which tends to be minimal and transient. However, we should note that extrusion becomes more significant at least in the initial stages of the process, especially when larger polymers are more mobile ($n=1$) and for very small x_{in}.

A. Dependence of polymerization on input rate

Figure 3(a) shows for $n=4$ the total length (per pore) of polymers fully or partially within the pore, l_{total}, as a function of x_{in}. Note that l_{total} effectively measures the total amount of polymerization. The variation with reaction time of l_{total} is also shown. At least for shorter times, the amount of polymerization increases monotonically with increasing monomer input rate x_{in}. Indeed, after a short transient, but still for early times, the rate of production of new polymers is proportional to x_{in}^2. However, for long reaction times, the amount of polymerization does not vary monotonically with x_{in}. Above a critical value, x_{in}^*, corresponding to the peak in the plot, the total length of polymer decreases with increasing x_{in} at least for a limited range. Higher x_{in} apparently induces too rapid clogging which inhibits further polymer growth. Lower x_{in} allows polymers to form and diffuse deeper inside the pores, so that a larger number of polymers can more readily form.

Another perspective on the above behavior comes from consideration of the dependence on x_{in} of average number of polymers that remain in each pore, N_p, after certain reaction time [see Fig. 3(b)]. For small x_{in}, the number is low so that most of the pores are unoccupied. For large x_{in}, most of the pores contain two polymers with locations concentrated near the two ends of the pore. The number of polymers reaches a maximal value around 3 at around $x_{in}=x_{in}^*$ corresponding to the maximum in the amount of polymerization in Fig. 3(a).

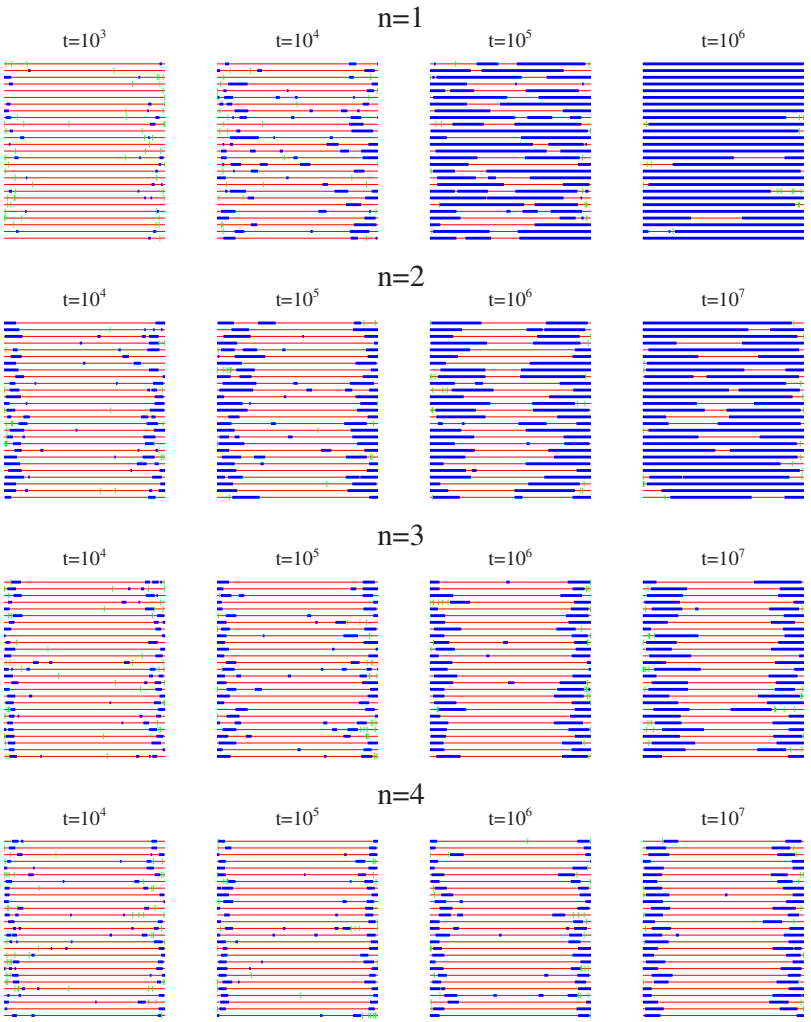

FIG. 2. (Color online) Snapshots of polymer distributions within mesopores after various reaction times (shown). Blue (narrower and darker) segments indicate polymers and green (wider and lighter) segments indicate monomers. The diffusion rate for a polymer of length l is $h(l)=h_m/l^n$, with $n=1$, 2, 3, and 4 from top to bottom rows. The monomer intake rate is $x_{\text{in}}=0.1$.

Finally, we contrast behavior described above for $n=4$ with that for $n=1$ where longer polymers are far more mobile. Results in Fig. 4 show that for the latter ($n=1$), there still appears a peak at some x_{in}^* in the mean number of polymers per pore versus input rate (shifted to somewhat higher x_{in} compared to $n=4$). However, no peak is evident in the total polymer length in the simulated range of x_{in} (although there appears a shoulder in l_{total} near x_{in}^*). This is not surprising as the enhanced mobility of longer monomers (relative to the case $n=4$) reduces the potential for rapid clogging.

B. Dynamics of the mean polymer length

Next, in Fig. 5, we show the evolution with reaction time of the average length of polymers, l_{av}, for $x_{\text{in}}=0.1$. We find quite good scaling with time of the form $l_{\text{av}}\sim t^{\gamma}$ for $n\geq 2$, where it appears that $\gamma\approx 1/(n+1)$. For $n=1$, i.e., more mobile longer polymers, time evolution is less well described by such scaling and the effective γ appears larger than the above prediction. We now elucidate this behavior.

For larger $n\geq 2$ where longer polymers are relatively immobile, one anticipates that most of the increase in total polymer length is associated with monomers aggregating with polymers rather than polymer-polymer aggregation. To analyze this behavior, we consider the regime of moderate x_{in} and where the density of catalytic sites which is not too high (conditions discussed further in the Appendix). Furthermore, we shall ignore the transient regime where monomers initially enter the pore and polymerization is initiated. Instead, we shall consider the subsequent regime where (i) a reasonably long polymer has formed near each end of the pore, (ii) the monomer density in the interior region is negligible, and (iii) growth of the polymer is controlled by monomers fed from the exterior reacting with the end of the polymer which is within but typically near the pore opening.

After each polymerization reaction, the end of the long polymer is shifted one site away from a reactive catalytic site. Thereafter, this end of the polymer undergoes a random walk in 1D. Thus, a key issue is how long does it take for the end of the long polymer to return to that catalytic site or to diffuse to a neighboring site (at which time a polymerization reaction will occur with finite probability which we denote by P_{rx}). Due to the intrinsic nature of a 1D random walk, the end of the polymer is actually far more likely to return to the same catalytic site (after a number of hops satisfying $n_h\sim l_c$) rather than to first reach a neighboring catalytic site (after a number of hops satisfying $n_h\sim l_c^2$) [23–26]. Even more relevant for our analysis is that the mean number of hops to reach any catalytic site for the 1D problem satisfies $\langle n_h\rangle\approx l_c$ [24]. Next, we assess the probability of reaction,

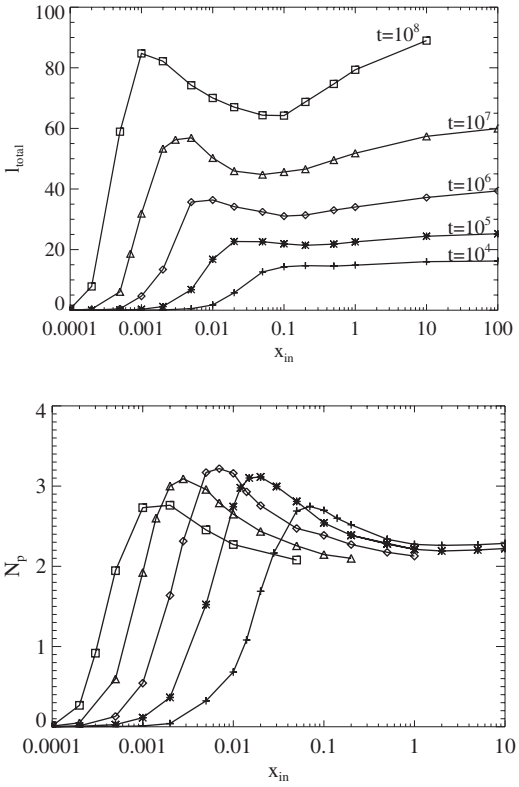

FIG. 3. (a) The total length of polymers per pore and (b) the number of polymers per pore, as a function of monomer intake rate, x_{in}. Behavior is shown for different reaction times t. The scaling exponent for polymer diffusivity is $n=4$. Data shown are for $t=10^4(+)$, $10^5(*)$, 10^6 (diamonds), 10^7 (triangles), and 10^8 (squares).

$P_{\text{rx}}<1$, noting that only a finite fraction of sites which are not blocked by polymers are occupied by monomers. This fractional occupation should scale like $c_{\text{eq}}\approx x_{\text{in}}/h_m=x_{\text{in}}$ which is typically quite small. However, it is also important to recognize that the residence time of the end of the long polymer at the catalytic site, $\tau_{\text{poly}}=1/h(l)$, far exceeds the characteristic time, $\tau_m=1/h_m=1$, for monomer hopping. Thus, even if c_{eq} is small, there is usually sufficient time for monomers to reach the catalytic site and react before the polymer hops. As a result, for typical conditions, one has that $P_{\text{rx}}\approx 1$ [27].

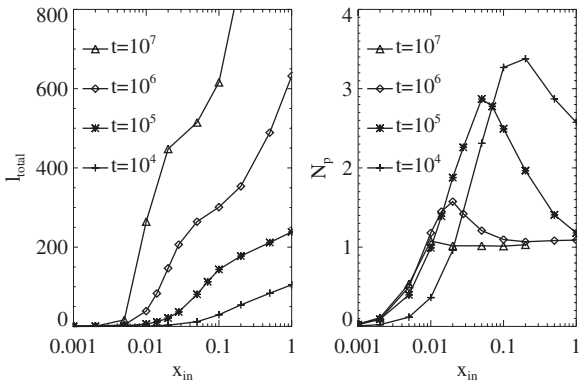

FIG. 4. Same as Fig. 3, but with polymer diffusion scaling exponent $n=1$. Data shown are for $t=10^4(+)$, $10^5(*)$, 10^6 (diamonds), and 10^7 (triangles).

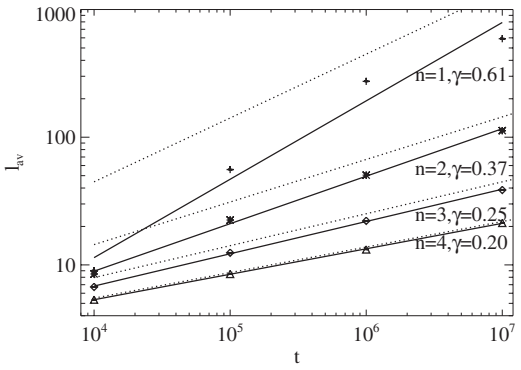

FIG. 5. Growth of average length of polymers for different size scaling exponents, n, for polymer diffusion for $x_{\text{in}}=0.1$. Symbols are simulation results and the lines are fit to power behavior t^{γ}. Dotted lines show the predictions of the analytic theory.

Since reaction of the end of the polymer chain with a monomer leads to growth of the length of the polymer by unity, based on the above analysis, one concludes that

$$\frac{d}{dt}l_{\text{av}} \approx P_{\text{rx}}h(l_{\text{av}})/\langle n_h\rangle \approx h_m/[l_c(l_{\text{av}})^n], \tag{1}$$

so that

$$l_{\text{av}} \approx [(n+1)(P_{\text{rx}}/l_c)(h_m t)]^{1/(n+1)} \approx [(n+1)t/l_c]^{1/(n+1)}, \tag{2}$$

consistent with $\gamma=1/(n+1)$ deduced from the above simulation results. More significantly, the result (2) for l_{av} recovers the simulated values with small error for larger n. One caveat is that this result is not as successful in all parameter regimes, an issue discussed further in the Appendix.

For $n=1$, there is significant mobility of larger polymers and thus polymer-polymer coalescence should be enhanced. In the extreme situation where growth of l_{av} is dominated by polymer-polymer coalescence, one would write $d/dtl_{\text{av}} \sim l_{\text{av}}h(l_{\text{av}})/l_c$ since each coalescence event increases the polymer length by an amount of order l_{av} (rather than by unity as for monomer-polymer coalescence). This would produce an exponent of $\gamma=1/n$ exceeding the above value. Presumably, this explains why the measured effective exponent for $n=1$ exceeds $\gamma=1/2$.

C. Polymer length distribution

Next, we consider the behavior of the polymer length distribution, $N(l)$, where $N(l)$ gives the number of polymers of length l per pore. Figure 6 shows the dependence of $N(l)$ on the scaling exponent, n, for polymer diffusivity (at reasonably long but fixed reaction time and at fixed input rate $x_{\text{in}}=0.1$). In all cases, the distribution is bimodal. At least for $n\geq 2$, the large-size peak reflects the distribution of lengths of the long polymers formed near each end of the pore at least. The small-size peak reflects a distribution of smaller polymers formed mainly in the interior of the pore in the early stages of polymerization. The identification of the larger and smaller size peaks is more ambiguous for $n=1$.

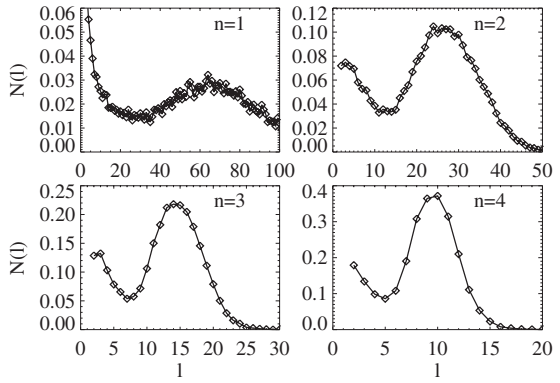

FIG. 6. Length distribution of polymers for different size scaling exponents, n, for polymer diffusion. The reaction time is 10^5 and the input rate is $x_{in}=0.1$.

Figure 7(a) shows the evolution of the polymer length distribution, $N(l)$, with reaction time for fixed $n=2$ and fixed $x_{in}=0.1$. One observes the relative growth of the large-size peak with time and the diminution of the small-size peak as the smaller polymers in the interior of the pore diffuse and coalesce (cf. the discussion above). Given the dynamic scaling of the average polymer length described above, it is natural to examine a rescaled form, F, of the polymer length distribution defined by $N(l) \propto F(l/l_{av})$. We choose the normalization constant so that $\int F(x)dx=1$. Then, the appropriate choice of l_{av} will ensure that $\int xF(x)dx=1$. The results in

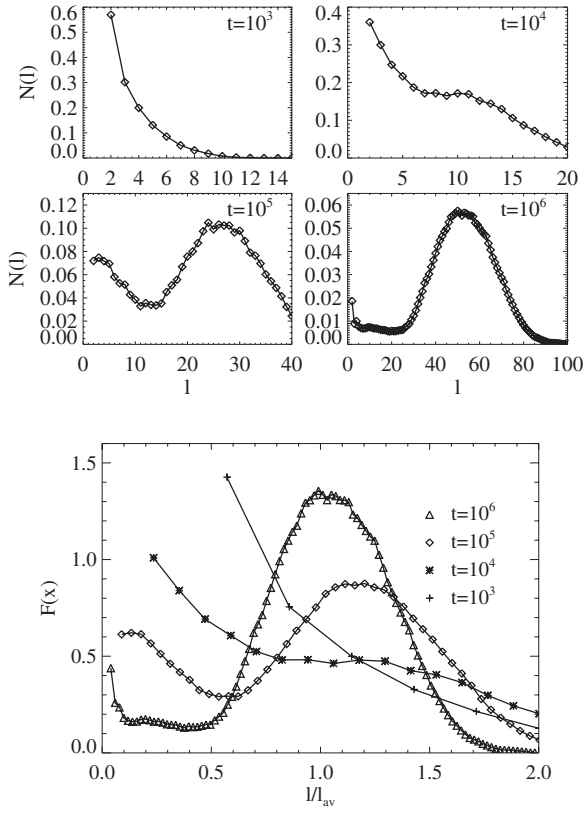

FIG. 7. (a) Length distribution of polymers for different reaction times t. The size scaling exponent for polymer diffusion is $n=2$ and $x_{in}=0.1$. (b) Scaling function, F, for the polymer length distribution.

Fig. 7 indicate that significant deviations from perfect dynamic scaling, i.e., there is no perfect collapse of curves for different times. This is not surprising since the growth dynamics of the longer polymers (associated with the large-size peak), which primarily control the behavior of l_{av}, is quite distinct from that of the smaller polymers.

Extracting a refined average length from the larger polymers in each pore and deconvoluting the large-length peak from the full polymer length distribution produce somewhat better dynamic scaling for the single peak corresponding to the longer polymers. One could consider a simple Markovian master-equation-type description of evolution of this component of the polymer length distribution due to monomer-polymer aggregation. However, this formulation predicts a strong sharpening in time of the rescaled form of the polymer length distribution not observed in the simulations. Thus, a more complex non-Markovian formulation is required to describe this distribution which accounts for the details of the return time distribution for the end of a polymer to a catalytic site. This technical analysis will be presented separately.

IV. DEPENDENCE OF POLYMERIZATION KINETICS ON OTHER MODEL PARAMETERS

In this section, we briefly describe the dependence of model behavior on a few basic model parameters such as the pore length, the number or density of catalytic sites, and on a finite (rather than infinite) microscopic rate, k, for the polymerization reaction. Polymer length distributions with varying pore lengths are plotted in Fig. 8 after a fixed reaction time. With relatively fast polymer diffusion ($n \leq 2$), behavior of polymer polymerization is somewhat sensitive to the pore length, with longer pores producing more separated bimodal distributions. Note that with longer pores, it takes longer for the system to reach the scaling regime.

One might anticipate that model behavior is relatively insensitive to the length of the pores for $n \geq 2$ (keeping l_c constant) since most of the polymerizations occur near the pore openings. This feature is confirmed in Fig. 8(b) which shows the dependence of the polymer length distribution on pore length for $n=4$. There is an increase in the small-length peak with increasing pore length due to a larger number of small polymers in the interior of the pore. However, the distribution also quickly converges to a limiting form for $L \to \infty$.

There is also some relatively mild variation of the polymer length distribution with the number of catalytic sites. Fewer catalytic sites results in an increase in the relative population of smaller polymers (see Fig. 9 for the case of $n=3$). Typically, shorter polymers are formed in the middle of the pore, while larger polymers are formed at the ends of the pore. With less catalytic sites, more polymers are formed or can diffuse to the middle of the pores, thus increase the proportion of smaller polymers.

Finally, we consider the effect of finite (rather than infinite) microscopic rate for polymerization, i.e., we set $k_1=k_2=k_3=k<\infty$. Results for different k values while fixing other parameters are shown in Fig. 10 (for $n=2$; results for other n values are very similar). For small values of k, the

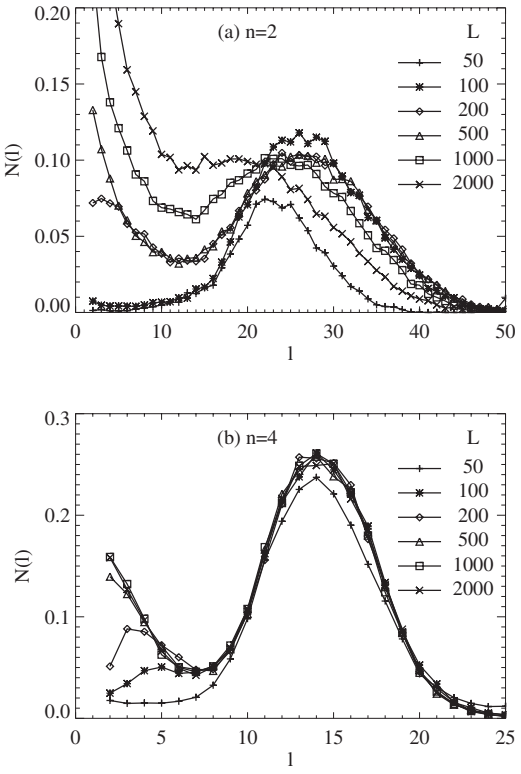

FIG. 8. Polymer length distribution vs pore length L. We choose (a) a size scaling exponent of $n=4$, a reaction time of $t=10^6$, and (b) a size scaling exponent of $n=2$, a reaction time of $t=10^5$. For both sets of figures, we choose a reaction rate of $k=\infty$, an input rate of $x_{\text{in}}=0.1$, and retain constant $l_c=10$.

bimodal nature of the polymer length distribution is eliminated. This is not surprising since reduced polymerization rate relative to diffusion rates will reduce the tendency to form large polymers, particularly near the openings of the pore. However, it should be noted that a significant change on the polymer length distribution from the case of instantaneous reaction occurs only for the regime $k<1$.

V. SUMMARY

In this study, we have analyzed both the spatial and temporal aspects of polymerization reactions within mesopores.

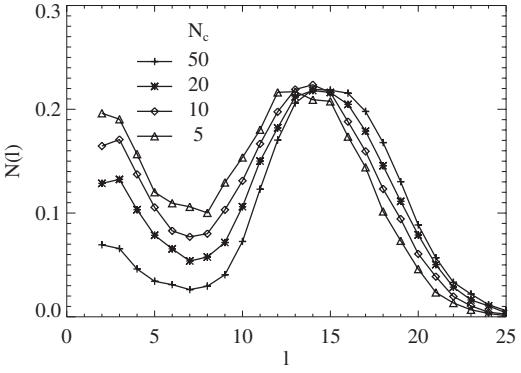

FIG. 9. Polymer length distribution for different numbers of catalytic sites, N_c, within each pore of length $L=200$. Other parameters are $n=3$, a reaction rate of $k=\infty$, a reaction time of 10^5, and $x_{\text{in}}=0.1$.

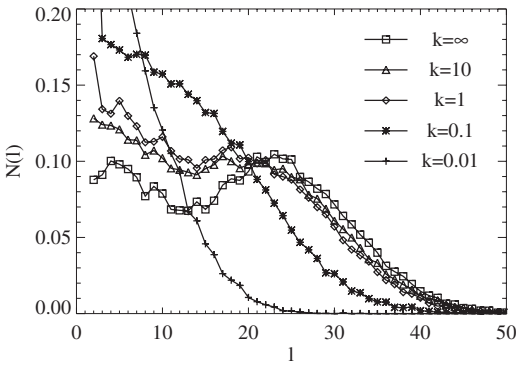

FIG. 10. Polymer length distribution for various polymerization rates k of 0.01 (pluses), 0.1 (asterisks), 1 (diamonds), 10 (triangles), and ∞ (squares). Other parameters are $n=2$, reaction time 10^5, and $x_{\text{in}}=0.05$.

A lattice-gas model was developed to capture the key features of this process, while allowing efficient analysis of its behavior through kinetic Monte Carlo simulation. A specific challenge was to analyze the interplay between the one-dimensional transport dynamics for monomers and polymers within the pores and the catalyzed reaction kinetics. Under typical conditions, the system operates in a clogging regime where longer polymers tend to form and grow near the ends of the pores primarily due to monomer-polymer aggregation for $n\geq 2$. Based on this observation, we are able to develop a successful analytic theory to describe the growth dynamics of the mean polymer length. To this end, we exploited results from the theory of 1D random walks and in particular results for random walks in the presence of traps.

This type of polymerization model is readily amenable to modification to treat a variety of different scenarios and systems. For example, one could drop the constraint of "single-file" diffusion by allowing monomers and polymers to diffuse along a small number of parallel coupled linear lattices within the pore [28]. This would allow some monomers to bypass polymers and reach the interior of the pore, undoubtedly significantly impacting the polymerization kinetics.

ACKNOWLEDGMENTS

This work was supported by the Division of Chemical Sciences, Office of Basic Energy Sciences of the U.S. Department of Energy (USDOE). It was performed at Ames Laboratory which is operated for the USDOE by Iowa State University under Contract No. DE-AC02-07CH11358.

APPENDIX: GROWTH DYNAMICS OF THE MEAN POLYMER LENGTH

Simulations presented earlier show a $t^{1/(n+1)}$ behavior for average length of polymers that remain inside a pore after reaction time t. Results of a more comprehensive analysis varying both x_{in} and the mean separation between catalytic sites, l_c (but retaining $n=4$), are shown in Fig. 11.

We now enumerate a few key observations from Fig. 11 in addition to providing some explanations of this behavior:

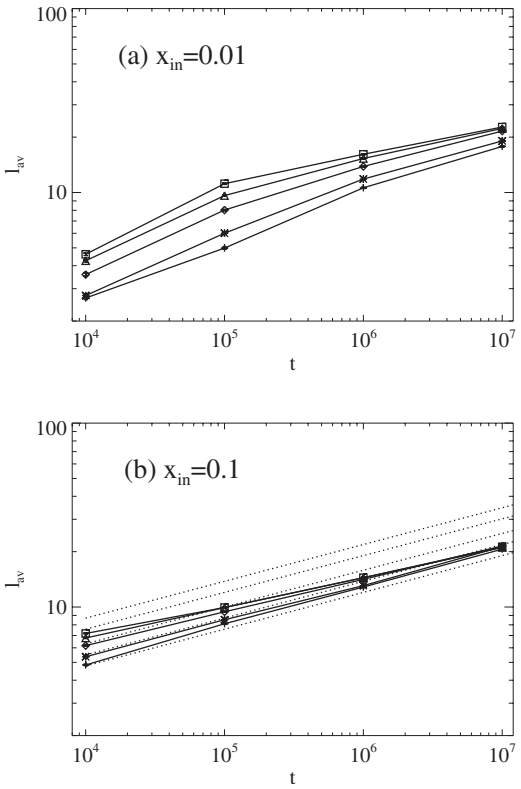

FIG. 11. Growth of the average length of polymers that remain inside a pore with the reaction time t for $n=4$. Symbols show results for different concentrations of catalytic sites corresponding to average separations of $l_c=20(+)$, $10(*)$, 5 (diamonds), 2 (triangles), and 1 (squares). The monomer intake rates (a) $x_{\text{in}}=0.01$ and (b) 0.1. Dotted lines in (b) are analytic predictions from Eq. (2).

(i) For smaller x_{in}, the regime of "good" temporal scaling is delayed until much later reaction times. This is readily understood since for smaller x_{in}, one expects that clogging of pores by a longer polymer near the ends and subsequent growth primarily by monomer-polymer aggregation occur much later.

(ii) There is a fundamental discrepancy between the prediction of the analytic theory in Sec. III C and the simulation results for higher densities of catalytic sites (i.e., smaller separations, l_c) at least for longer reaction times. Specifically, values of l_{av} for different l_c seem to converge at long times.

(iii) This deviation from the analytic prediction is related to the feature that for high densities of catalytic sites and long times, there is a tendency for the long polymer to become partly extruded from the pore. Our analytic treatment did not consider this scenario. In this regime, polymer growth is limited by how often the polymer can diffuse back completely inside the pore, which is independent of the density of catalytic sites.

(iv) The case where $l_c=1$ (i.e., all lattice sites are catalytic) constitutes an extreme example of the above scenario and deviates from our analytic theory even for short reaction times. Here, a long polymer grows rapidly toward the end of the pore by incorporating every monomer which reaches its end. Thus, very quickly the end of the polymer reaches the end of the pore. Again, the end of the polymer can diffuse out of the pore and one must wait for it to return inside the pore for further growth.

A more detailed analysis of the extreme case $l_c=1$ is instructive. From Fig. 11 for $x_{\text{in}}=0.1$, a distinct scaling behavior with exponent $\gamma\approx 0.16$ is observed for $n=4$. To explain this behavior, we assume that $P_{\text{rx}}\approx 1$ (i.e., polymer growth occurs rapidly as soon as the end of the growing polymer is inside the pore). Then, after each polymerization event where the end of the polymer is at the end of the pore, there are two possibilities: Either the end of the polymer can diffuse deeper within the pore leading to further polymer growth which quickly returns the end of the polymer to the end of the pore. Alternatively, it can diffuse outside of the pore in which case further growth by at least one monomer only occurs if and when the end of the polymer returns within the end of the pore. (Such return becomes increasingly likely as the polymer grows since the probability of the polymer being completely extruded is given by the reciprocal of its length [29].)

Considering the one-dimensional random walk of the end of the partly extruded polymer, the average number of returns to the end of the pore (and thus the average length of the polymer) should scale like the square root of the total number of hops up to the current time, t [23,24]. Thus, one concludes that $l_{\text{av}}(t)^2$ should scale like $\int_0^t dt' h[l_{\text{av}}(t')]$. Using $h(l)\sim l^{-n}$, we conclude that this integral relation implies the scaling $l_{\text{av}}\sim t^{1/(n+2)}$. This behavior is distinct from that described in Sec. III B, but consistent with above simulation result for $n=4$. We have also confirmed its validity for other $n\geq 2$ when $l_c=1$.

[1] K. Tajima and T. Aida, *Nanostructured Catalysts* (Plenum, New York, 2003).
[2] J. S. Beck *et al.*, J. Am. Chem. Soc. **114**, 10834 (1992).
[3] M. de Fátima V. Marques, O. F. C. da Silva, A. C. S. L. S. Coutinho, and A. S. de Araujo, Polym. Bull. (Berlin) **61**, 415 (2008).
[4] F. Márquez, R. Roque-Malherbe, J. Ducongé, and W. del Valle, Surf. Interface Anal. **36**, 1060 (2004).
[5] V. S.-Y. Lin, D. R. Radu, M.-K. Han, W. Deng, S. Kuroki, B. H. Shanks, and M. Pruski, J. Am. Chem. Soc. **124**, 9040 (2002).
[6] K. Kageyama, J. Tamazawa, and T. Aida, Science **285**, 2113 (1999).
[7] T. P. Nevell and S. H. Zeronian, *Cellulose Chemistry and Its Applications* (Ellis Horwood, New York, 1985), Chap. 2.
[8] S. Huh, J. W. Wiench, J.-C. Yoo, M. Pruski, and V. S.-Y. Lin, Chem. Mater. **15**, 4247 (2003).
[9] J. Kärger and D. Freude, Chem. Eng. Technol. **25**, 769 (2002).
[10] L. Lizana and T. Ambjörnsson, Phys. Rev. Lett. **100**, 200601 (2008).

[11] F. Marchesoni and A. Taloni, Phys. Rev. Lett. **97**, 106101 (2006).
[12] C. Lutz, M. Kollmann, and C. Bechinger, Phys. Rev. Lett. **93**, 026001 (2004).
[13] S. V. Nedea, A. P. J. Jansen, J. J. Lukkien, and P. A. J. Hilbers, Phys. Rev. E **65**, 066701 (2002).
[14] A. P. J. Jansen, S. V. Nedea, and J. J. Lukkien, Phys. Rev. E **67**, 036104 (2003).
[15] S. V. Nedea, A. P. J. Jansen, J. J. Lukkien, and P. A. J. Hilbers, Phys. Rev. E **67**, 046707 (2003).
[16] R. M. Ziff, E. Gulari, and Y. Barshad, Phys. Rev. Lett. **56**, 2553 (1986).
[17] K. A. Fichthorn and W. H. Weinberg, J. Chem. Phys. **95**, 1090 (1991).
[18] J. W. Evans, D.-J. Liu, and M. Tammaro, Chaos **12**, 131 (2002).
[19] A. Baumgärtner and M. Muthukumar, J. Chem. Phys. **87**, 3082 (1987).
[20] V. Yamakov and A. Milchev, Phys. Rev. E **55**, 1704 (1997).
[21] D. Dubbeldam, S. Calero, T. L. M. Maesen, and B. Smit, Phys. Rev. Lett. **90**, 245901 (2003).
[22] D. S. Sholl and K. A. Fichthorn, Phys. Rev. Lett. **79**, 3569 (1997).
[23] B. D. Hughes, *Random Walks and Random Environments Vol. 1: Random Walks* (Clarendon, Oxford, 1995).
[24] E. W. Montroll and G. H. Weiss, J. Math. Phys. **6**, 167 (1965).
[25] K. E. Shuler, H. Silver, and K. Lindenberg, J. Stat. Phys. **15**, 393 (1976).
[26] The preference to return to the same trap in a periodic array of traps would be diminished in higher dimensions.
[27] A more detailed analysis estimates the probability of no reaction while the end of the polymer is at the catalytic site as $1-P_{\mathrm{rx}}=(1-c_{\mathrm{eq}})^{\tau_{\mathrm{poly}}/\tau_m}$.
[28] E. B. Stukalin and A. B. Kolomeisky, J. Chem. Phys. **124**, 204901 (2006).
[29] D.-J. Liu and J. W. Evans, Phys. Rev. B **66**, 165407 (2002). The stated result follows from the analysis in the Appendix of a 1D random walk between traps.